JOURNAL OF Applied Polymer SCIENCE

The Thermal Properties of a Carbon Nanotube-Enriched Epoxy: Thermal Conductivity, Curing, and Degradation Kinetics

Isaac Aguilar Ventura, Ariful Rahaman, Gilles Lubineau
COHMAS Laboratory, Physical Science and Engineering Division, King Abdullah University of Science and Technology (KAUST), Thuwal 23955-6900, Saudi Arabia
Correspondence to: Gilles Lubineau (E-mail: gilles.lubineau@kaust.edu.sa)

ABSTRACT: Multiwalled carbon nanotube-enriched epoxy polymers were prepared by solvent evaporation based on a commercially available epoxy system and functionalized multiwalled carbon nanotubes (COOH–MWCNTs). Three weight ratio configurations (0.05, 0.5, and 1.0 wt %) of COOH–MWCNTs were considered and compared with neat epoxy and ethanol-treated epoxy to investigate the effects of nano enrichment and processing. Here, the thermal properties of the epoxy polymers, including curing kinetics, thermal conductivity, and degradation kinetics were studied. Introducing the MWCNTs increased the curing activation energy as revealed by differential scanning calorimetry. The final thermal conductivity of the 0.5 and 1.0 wt % MWCNT-enriched epoxy samples measured by laser flash technique increased by up to 15% compared with the neat material. The activation energy of the degradation process, investigated by thermogravimetric analysis, was found to increase with increasing CNT content, suggesting that the addition of MWCNTs improved the thermal stability of the epoxy polymers. © 2013 Wiley Periodicals, Inc. J. Appl. Polym. Sci. 130: 2722–2733, 2013

KEYWORDS: composites; thermal properties; thermogravimetric analysis; differential scanning calorimetry; nanotubes; graphene and fullerenes

Received 8 October 2012; accepted 16 April 2013; Published online 31 May 2013
DOI: 10.1002/app.39438

INTRODUCTION

Epoxy resins are widely used thermoset polymers for high-performance applications (e.g., as coatings, adhesives, and matrices for fiber-reinforced composites) because of their good mechanical properties, excellent adhesion, and good chemical and heat resistance. However, new applications require improvements for these properties. Doping bulk epoxy resins with even a very small content of carbon nanotubes (CNT) can significantly modify their properties.[1–3] Most past studies focused on investigating the mechanical, thermal, or electrical properties of such enriched epoxy polymers.[4–10] It has been shown that these properties depend on the nanoparticle dispersion and CNT–polymer interactions,[11,12] therefore, research has also taken a particular interest in surface functionalization.

Yet, CNTs not only affect the final behavior of a polymer but also its curing process. On top of classical processing factors, such as the curing cycle (temperature, time, and pressure) and the resin-to-curing agent ratio, the contents of the CNTs are an added parameter that can significantly affect the curing kinetics. Moreover, two other important thermal characteristics can be changed with the addition of CNTs to the epoxy: the thermal conductivity and the degradation kinetics.

Puglia et al.[13] studied the effects of single-walled carbon nanotubes (SWCNTs; 5 wt % and 10 wt %) on the curing reaction of diglycidyl ether of bisphenol A (DGEBA)/diethylene triamine (DETA) under dynamic and isothermal conditions. They reported that the rate of reaction was accelerated in the presence of SWCNTs. Xie et al.[14] reported that incorporating 1 wt % multiwalled carbon nanotubes (MWCNTs) induced a slight catalytic effect on the curing behavior of the epoxy, while incorporating 5 wt % MWCNTs significantly accelerated the curing. They reported this acceleration to be negligible in the case of carbon nanofibers even at a high weight ratio (1 wt % and 5 wt %).[15] Meanwhile, Choi et al.[16] reported that the presence of MWCNTs delayed the curing of an epoxy resin. Most of the research in this area has focused on curing behaviors of CNT–epoxy systems with high concentrations of CNTs (>1 wt %)[13,14,17] while there have been few studies that have reported on curing behaviors with low concentrations of CNTs.[18] Yet, understanding the changes of curing behaviors at very low concentrations of CNTs (<1 wt %) is of high practical interest. Indeed, it has been shown that the threshold level for improving the electrical or thermal conductivity of an epoxy can be achieved at concentrations as low as 0.5 wt % MWCNTs.[1,19]

In general, an epoxy is insulator and a poor thermal conductor (thermal conductivity $\approx$ 0.18 W mK^{-1}).[19] To provide thermal transfer, carbon nanotubes have been used as fillers in epoxy composites due to their high thermal conductivity. Assael et al.[20] used the transient hot wire technique to study the thermal conductivity of a nano-enriched epoxy at room temperature. They observed that the addition of 2 wt % of MWCNT fillers increased the thermal conductivity of the composite by 9%. Song et al.[1] reported clear experimental evidence of the major role of dispersion in epoxies enriched with 1.5 wt % CNTs.

The study of thermal stability is critical for engineering polymers since the material's range of safe operating conditions is directly related to the thermal degradation behavior. To evaluate the thermal stability, it is necessary to measure parameters such as initial decomposition temperature, the temperature at which the degradation rate is highest, and the activation energy of the degradation reaction.[21,22] Thermal stability of MWCNT-enriched epoxies containing 0.1 wt % to 2 wt % MWCNTs were investigated by Chen et al.[7] The initial degradation temperature clearly increased with an increase in the CNT load from 0.1 wt % to 2 wt %. Zhou et al.[23] reported that the thermal decomposition temperature of an epoxy decreased with increased CNT content. Jin et al.[24] studied the thermal properties of epoxy–CNT composites. They also reported a decrease in the thermal stability in the presence of MWCNTs. This decrease became negligible when functionalized CNTs were used. While the global degradation process of epoxy–CNT composites has been intensively investigated using thermogravimetric analysis, the degradation kinetics has had little attention.

The objective of this study is to investigate the effects of low MWCNT contents (<1 wt %) on the curing kinetics, thermal conductivity, and thermal degradation kinetics of the MWCNT-enriched epoxies. To meet this objective, we studied the morphology of MWCNT–epoxy composites using high-resolution transmission electron microscopy (HR-TEM). We identified the chemical groups using Fourier transform infrared spectroscopy (FTIR) analysis. We characterized the CNT–epoxy composites via their curing properties, including the temperature of the maximum rate of polymerization (T_p), the onset temperature (T_i), the activation energy of the polymerization reaction (E_a), and their degradation properties, including the initial degradation temperature (T_I) the temperature of the maximum rate of weight loss (T_M), and the activation energy of the degradation reaction (E_d^{rd}).

EXPERIMENTAL

The Material System

We prepared MWCNT-enriched epoxies using the following raw materials:

- —COOH functionalized MWCNTs were obtained from Cheap Tubes (Brattleboro, VT) and produced by catalyzed chemical vapor deposition. According to the supplier's specifications, the purity was higher than 95 wt %, the residual ash was less than 1.5 wt % and the concentration of —COOH groups was 2.56 wt % of TGA analysis on functionalized MWCNT confirmed that the concentration of —COOH is approximately 2.15 $\pm$ 0.15 wt %. The as-received dimensions (outer diameter from 8 to 15 nm, inner diameter from 3 to 5 nm, length from 10 to 50 μm) were confirmed by HR-TEM observations [Figure 1(a)]. The Raman spectrum of these MWCNTs [Figure 1(b)] was obtained using a LabRAM HR 800 Raman spectrometer (Horiba Co.) with a range from 200 to 3500 cm^{-1}. The D-band, G-band, and G′-band appeared as expected at 1350, 1580, and 2710 cm^{-1}, respectively. The relative intensity (D/G) between the D and the G bands is known to be a good indicator of the quantity of the structural defects within MWCNTs. Usually, the intensity of the D-band largely increases with the presence of amorphous carbon or defects created during the addition of the functional groups in the sidewall.[25,26] The intense D-band in this spectrum indicates that these MWCNTs obviously contained multiple structural defects due to their functionalization.[27,28]
- EPOLAM 2063, supplied by AXSON Technologies, is a commercially available product that is based on a blend of cycloaliphatic epoxy resin (CA) and a diglycidyl ether of bisphenol-A (DGEBA) resin. We mixed it with a compatible curing agent (anhydride 1,2,3,6-tetrahydromethyl-3,6-methanophtalique) in equal parts by volume. According to the supplier's

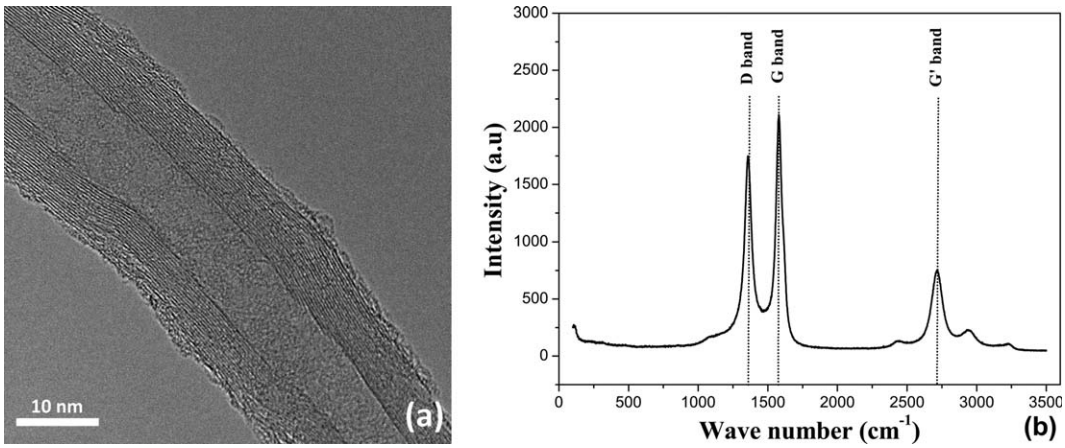

Figure 1. (a) HR-TEM image of the MWCNTs and (b) Raman spectrum of the MWCNTs.

Applied Polymer SCIENCE

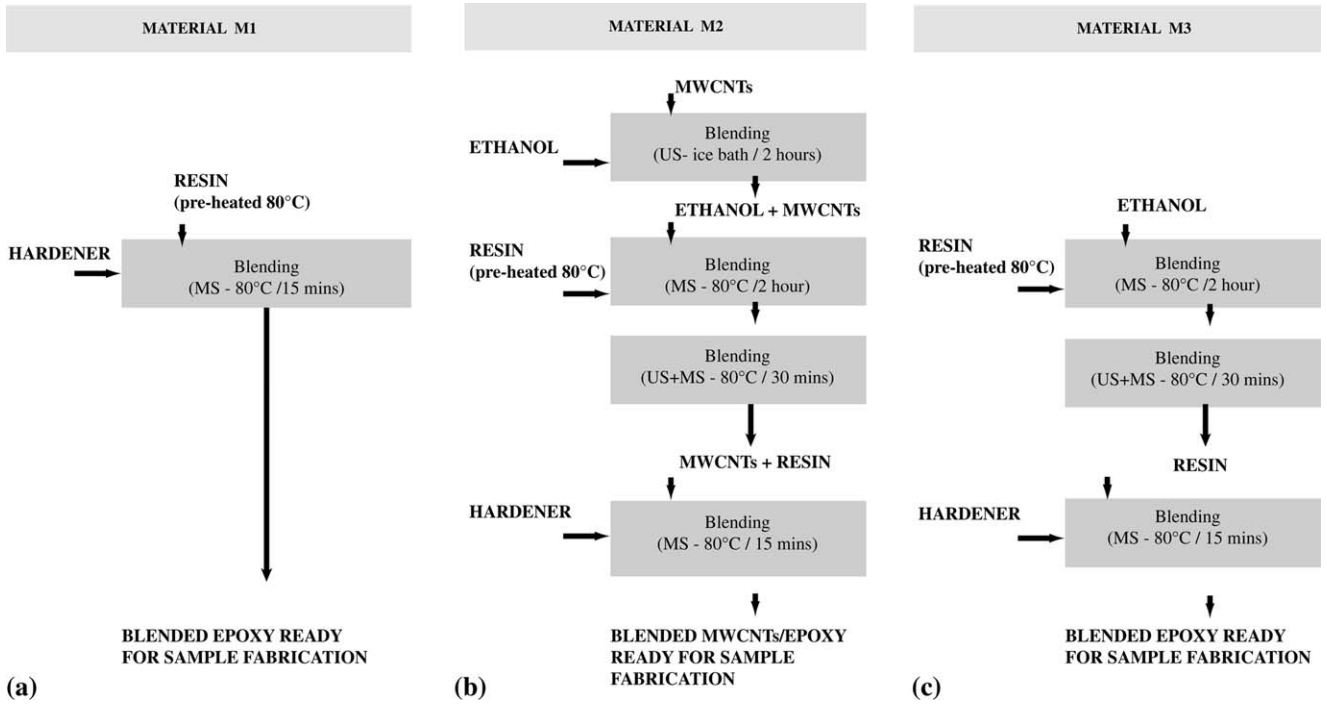

Figure 2. Flowchart of the processing technique for materials: (a) M1, (b) M2, (c) M3. MS = Magnetic stirring, US = Ultra-sonication. [Color figure can be viewed in the online issue, which is available at wileyonlinelibrary.com.]

specifications, the tensile strength and Young's modulus of this epoxy are 57 MPa and 3.1 GPa, respectively, at 23°C. The glass transition temperature is expected to range from 180°C to 200°C depending on the curing cycle.

Preparation

Three different material configurations, labeled as M1, M2, and M3, were studied. A flowchart describing the key steps of the processing technique is provided in Figure 2 for each of these material configurations.

Material M1 [Figure 2(a)] is the reference configuration. The epoxy resin was heated to 80°C to reduce the viscosity. The required amount of curing agent was added (ratio of 5 : 5.35 by weight as prescribed by the supplier) and stirred using a magnetic stirrer for 15 min at 80°C.

Material M2 [Figure 2(b)] is the epoxy resin mixed with the MWCNTs and denoted M2-0.05, M2-0.5, and M2-1.0 according to the 0.05, 0.5, and 1.0 wt% MWCNT contents with respect to the total weight of the resin and curing agent. The MWCNTs were first dispersed into ethanol (1/11 wt % of ethanol in the total resin/curing agent mixture) by sonication (Sonicator: CPX500 Cole-Parmer Instruments, frequency: 20 kHz) for 2 h in an ice bath. Then, the MWCNT–ethanol solution was added to the epoxy (preheated to 80°C); this mixture was stirred continuously using a magnetic stirrer for 2 h at 80°C until all the ethanol evaporated. Afterward, the mixture was sonicated and simultaneously stirred using a magnetic stirrer for 30 min at 80°C. In the next step, the corresponding amount of curing agent was added and the solution was thoroughly stirred for 15 min to yield a homogeneous mixture.

Material M3 [Figure 2(c)] was prepared exactly in the same way as material M2, except that no MWCNTs were added. The purpose of material M3 was to distinguish the effects of the addition of MWCNTs from the processing effects. For the thermal conductivity and thermal degradation kinetics measurements, all samples were prepared by moulding the epoxy resin in a 80°C preheated steel mold. The mold was kept at 80°C for 6 h followed by 6 h at 180°C to ensure complete curing of the samples (the extent of curing was checked by differential scanning calorimetry).

Characterization Techniques

The diameter of the MWCNTs and their dispersion into the resin was characterized using HR-TEM (TITAN TEM, FEI, with a point-to-point resolution of 0.24 nm). The MWCNTs were dispersed ultrasonically in an ethanol bath for 10 min. Finally, two drops of this liquid were dropped onto a carbon coated copper grid. The cured MWCNT-epoxy samples were cut into thin pieces (thickness: 50 nm) using microtome cutter and the pieces were collected onto a copper grid. For additional dispersion characterization, fractured surfaces of the MWCNT–epoxy composites were investigated using scanning electron microscopy (Nova Nano 630, FEI). The samples were coated with a thin layer of gold to reduce charging during analysis. The infrared spectra were recorded on a Perkin Elmer spectrum 100 FTIR using an attenuated total reflectance accessory. FTIR-ATR analysis of M1, M2, and M3 were performed in the frequency range of 4000–400 cm^{-1}.

- For the differential scanning calorimetry (DSC) analysis (Netzsch DSC 204 F1 calorimeter), uncured samples were

heated from 25°C to 250°C under pure nitrogen at respective heating rates of 3, 10, and 15°C min^{-1}. The experiments were performed in triplicate and the results were averaged. To identify the features of the curing process, we used a general kinetic model as described by eq. (1):

$$\frac{d\alpha}{dt} = kf(\alpha). \quad (1)$$

where k is the rate constant, α is the degree of conversion, and $f(\alpha)$ is a kinetic-dependent function. By assuming an Arrhenius dependency with temperature for the rate constant, eq. (1) can be classically rewritten as:

$$\frac{d\alpha}{dt} = A\exp\left(-\frac{E_a}{RT}\right)f(\alpha). \quad (2)$$

where A is the pre-exponential factor, E_a is the polymerization activation energy, and R is the gas constant. Following Friedman's isoconversional method,[29–31] eq. (2) can be reshaped as:

$$\ln\left(\frac{d\alpha}{dt}\right) = \left(-\frac{E_a}{R}\right)\frac{1}{T} + \ln\left(Af(\alpha)\right). \quad (3)$$

Then, for a given degree of conversion, E_a can be extracted from the slope of the relation. This method allows us to quantify the dependency of E_a with respect to the degree of conversion.

- The thermal conductivity K (W m^{-1} K^{-1}) was evaluated based on the thermal diffusivity λ(m^2 s^{-1}), the density ρ (kg m^{-3}), and the specific heat capacity c_p (J kg^{-1} K^{-1}):

$$K = \lambda \cdot \rho \cdot c \quad (4)$$

λ was measured using a LFA 447 laser ash diffusivity system. ρ was taken to be equal to 1160 kg m^{-3} (from the specification data sheet) and c_p was calculated using the DSC scan of the cured material. The measurement is repeated four times for each sample and the results presented are the average values.

- The thermogravimetry analysis (TGA) was carried out on fully cured samples using a Netzsch TG 209 F1 apparatus. All experiments were performed in triplicate and the results averaged. Weight loss was recorded under an N_2 atmosphere by increasing the temperature from 40 to 800°C at three different heating rates: 5, 10, and 15°C min^{-1}. These TGA data were then used to identify the activation energy for thermal decomposition (E_d^{rd}) by use of Kissinger's equation:[32,33]

$$-\ln\frac{\beta}{T_M^2} = \frac{E_d^{rd}}{RT_M} - \ln\frac{AR}{E_d^{rd}} \quad (5)$$

where β is the heating rate (°C min^{-1}), T_M is the most rapid degradation temperature (K), R is the gas constant (J mol^{-1} K^{-1}), and A is the pre-exponential factor.

RESULTS AND DISCUSSION

Characterization of Dispersion and Chemical Structure

Multiple TEM and SEM observations (Figure 3) show that the MWCNTs were efficiently dispersed in the resin. No clusters of MWCNTs were visible even at the maximum load of 1 wt %.

The reactions between the epoxy and anhydride curing agent in the M1 and M3 samples are shown in Figure 4(a). The anhydride groups of the curing agent did not directly react with the oxirane groups of DGEBA and CA.[34] Rather, the hydroxyl (–OH) groups of the epoxy (DGEBA) first reacted with the anhydride groups to form carboxylic (–COOH) groups (reaction-I). Then, these –COOH groups opened the oxirane groups of DGEBA and CA to produce hydroxyl groups (reaction-II and reaction-III). These –OH groups then reacted with the anhydride groups following reaction-I until all –OH groups participated in the curing reaction.

The reaction mechanism of the M2 sample is different, and is shown in Figure 4(b). Before any addition of the curing agent, the –COOH groups of the MWCNTs reacted with the oxirane groups of DGEBA and CA to form an epoxy-terminated prepolymer. Then, the reactions took place in the same manner as for M1. The hydroxyl groups of the terminated prepolymer reacted with the anhydride groups of the curing agent to produce the –COOH groups. It is clear that the MWCNTs created some initial cross-linking.

To observe the effect of the different reaction mechanisms on the final product, we performed FTIR analysis on all cured samples. The FTIR spectra provide information regarding changes in the sample at the molecular level through the displacement, widening, appearance or disappearance of bands. The detailed assignment of the absorption features is as follows: 2955–2869 cm^{-1} (–C–H of aromatic ring), 1785 cm^{-1} (anhydride –C=O), 1730 cm^{-1} (carboxylic acid –C=O), 1610 cm^{-1}, 1506 cm^{-1}, and 1450 cm^{-1} (stretching and deformation of aromatic –C=C), 1108 and 1038 cm^{-1} (deformation of aromatic –CH), 914 cm^{-1} (epoxide group).

It appears that the temporary addition of ethanol during the process does not modify the final material as revealed by the identical FTIR spectra of M1 and M3 (Figure 5). Characteristic absorption bands of carboxylic acid (–C=O) stretching vibrations at 1730 cm^{-1} and a C–H stretch at 2918 cm^{-1} were observed. The absence of an –OH stretching band at 3500–3200 cm^{-1} and an intense epoxy stretching vibration at 914 cm^{-1} confirmed that the epoxy groups were not totally consumed during the full polymerization process.[35,36]

As expected from the reaction mechanism, a modification to the chemical structure of the epoxy in the M2 samples was revealed by FTIR analysis. First, the absorption intensity of the band at 3500–3200 cm^{-1} is slightly increased, corresponding to an –OH stretch vibration of the –COOH group. Then, more –COOH groups are present in M2 samples compared with M1 and M3. These –COOH groups can be directly explained by the initial functionalization of the MWCNTs. Second, it can be clearly seen that the oxirane stretching frequency at 914 cm^{-1} disappears with respect to M1 and M3. This is due to the initial –COOH groups of the CNTs that start to consume the epoxy groups even before the addition of any curing agent. The direct consequence is that all active epoxy groups participate in the reaction in the M2 samples, either by direct reaction with the –COOH of the MWCNTs, or by classical reaction with the curing agent.

Applied Polymer SCIENCE

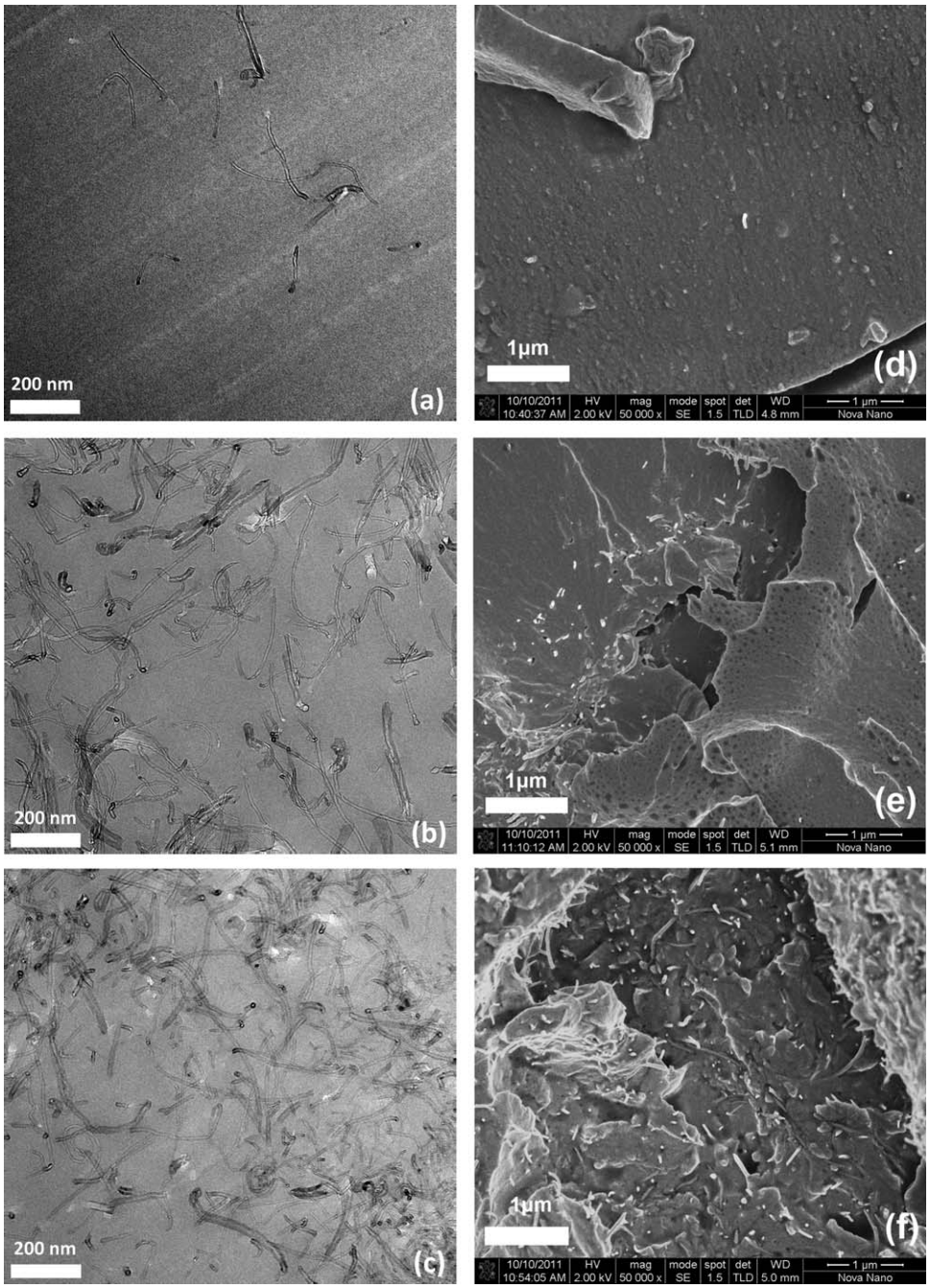

Figure 3. First column: TEM images of the MWCNT-modified epoxies. Second column: SEM images of fracture surfaces. (a,d) M2-0.05, (b,e) M2-0.5, and (c,f) M2-1.0.

Influence of the Content of the MWCNTs on the Curing Process

The dynamic DSC scans for the M1, M2-0.05, M2-0.5, M2-1.0, and M3 samples at a heating rate of 10°C min^{-1} are presented in Figure 6(a). Figure 6(b) shows average results from the M2-0.05 samples to illustrate some key features of the DSC curves: T_i is the onset temperature of intense polymerization, T_p is the temperature that corresponds to the maximum rate of polymerization, and ΔH is the total heat of reaction.

The key features that have been identified from the DSC scans at 3, 10, and 15°C min^{-1} are reported in Table I. T_i, T_p and ΔH can be considered identical in the M1 and M3 samples. An initial conclusion from these data is that the necessary modification of the process by the temporary addition of ethanol does not affect the curing process. In the CNT-enriched epoxies, we observe the following for each heating rate: (1) a slight decrease in the onset temperature, T_i; (2) a relatively stable exothermal peak temperature, T_p; and (3) a substantial decrease of the total

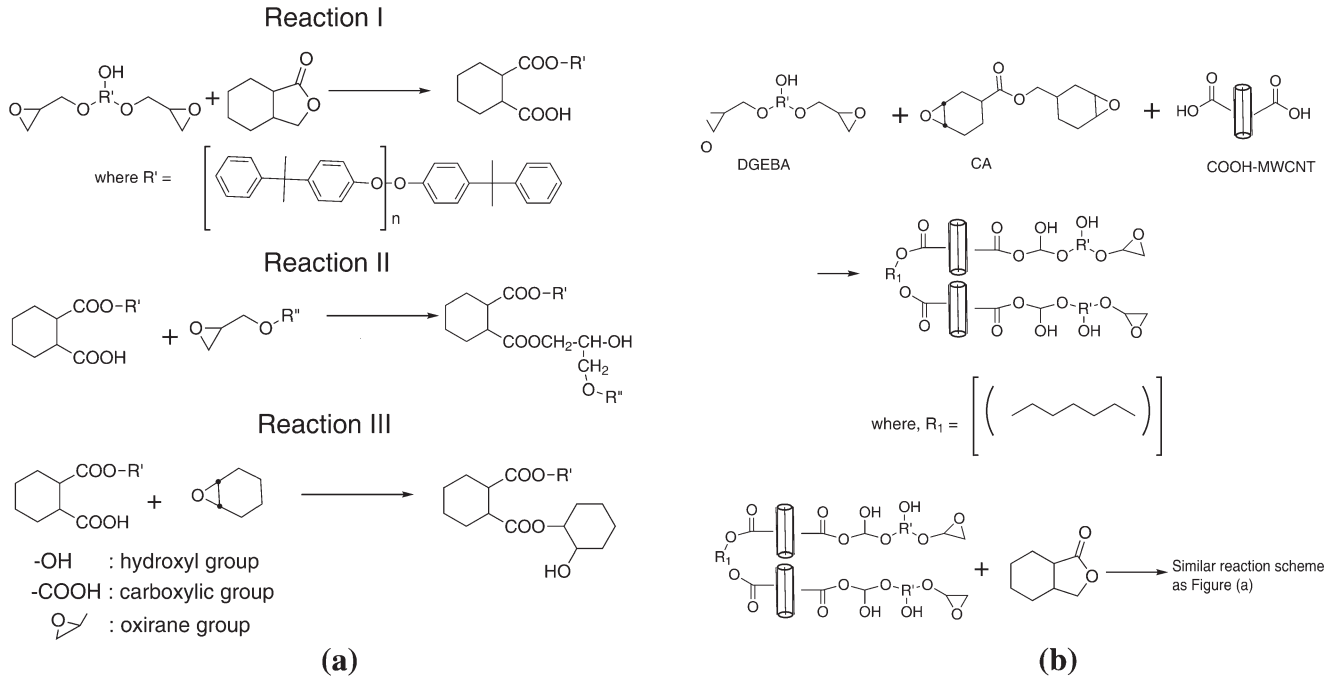

Figure 4. Reaction mechanisms. (a) Reaction between the epoxy and anhydride curing agent (M1 and M3). (b) Formation of the prepolymer and curing of the prepolymer (M2).

heat of reaction, ΔH. In multiple heating rate DSC scans, the apparent total heat of reaction tends to decrease with the heating rate.

We also identified the evolution of E_a during the curing process by use of isoconversional techniques. Figure 7 displays the degree of conversion α [Figure 7(a,c,e,g)] and the rate of conversion [Figure 7(b,d,f,h)] in relation to the temperature for the M1, M2-0.05, M2-0.5, M2-1.0 samples at three different heating rates (the results for M3 were similar to the results for M1 and are not shown). To estimate E_a at different degrees of conversion, the isoconversional temperatures are obtained from the cross points of the degree of conversion and the temperature [Figure 7(a,c,e,g)]. The slope $\left(-\frac{E_a}{R}\right)$ and the factor $\ln(Af(\alpha))$ of the $\frac{1}{T} \leftrightarrow \ln\left(\frac{d\alpha}{dt}\right)$ relation have been identified. Average values, as well as related statistics (range of variation and regression coefficient) are reported in Table II.

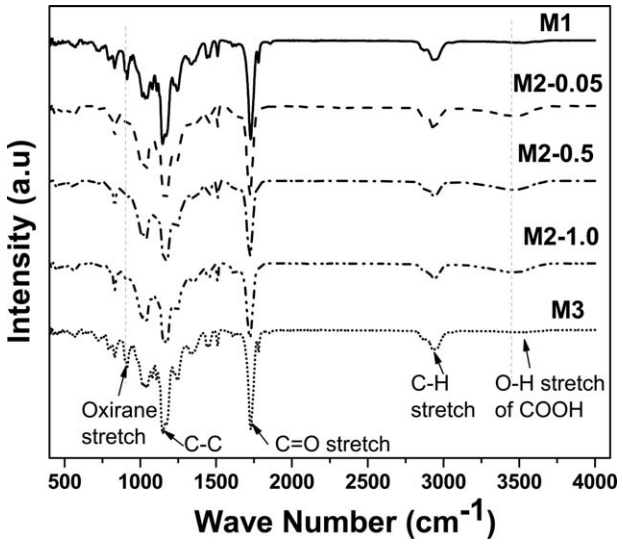

Figure 5. FTIR spectra for M1, M2-0.05, M2-0.5, M2-1.0, and M3.

The variation in E_a with the degree of conversion is reported in Figure 8 for each sample. E_a values for the M1, M2-0.05, M2-0.5, and M2-1.0 samples changed in the range of 60–88, 66–81, 67–80, and 69–83 kJ mol^{-1}, respectively, at different degrees of conversion ranging in between 0.15 and 0.90.

For M1, the evolution in activation energy might be associated with the progressive decrease of the polymer chains mobility. As the reaction progresses, the cross linking increases and the mobility of the unreacted groups decreases leading to an increase in the apparent activation energy.[37]

In the same way, the activation energy in M2 samples increases between $\alpha = 0$ to $\alpha = 0.6$ due to the chain mobility reduction with degree of curing. We have to note that the initial E_a ($\alpha = 0$) increases with respect to CNT content. This can be related to the initial reaction between the functionalized CNTs and the epoxy resin which reduced the mobility before any curing agent/epoxy reaction.

During the final stage of the reaction ($\alpha > 0.6$), the activation energy of the nanomodified samples decreases slightly while E_a of the reference material continues to increase.

Influence of the Content of the MWCNTs on Thermal Conductivity

The thermal conductivities obtained for the different material configurations are plotted in Figure 9. First, no modification was observed in the M1 and M3 samples. The temporary addition of ethanol during the process did not modify the thermal

Applied Polymer SCIENCE

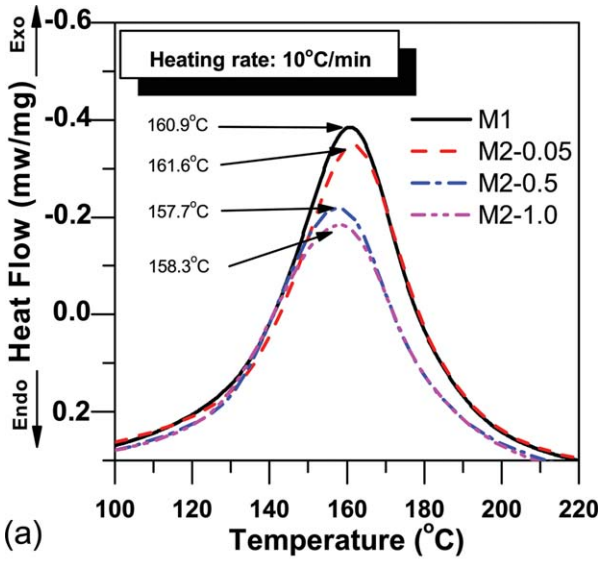

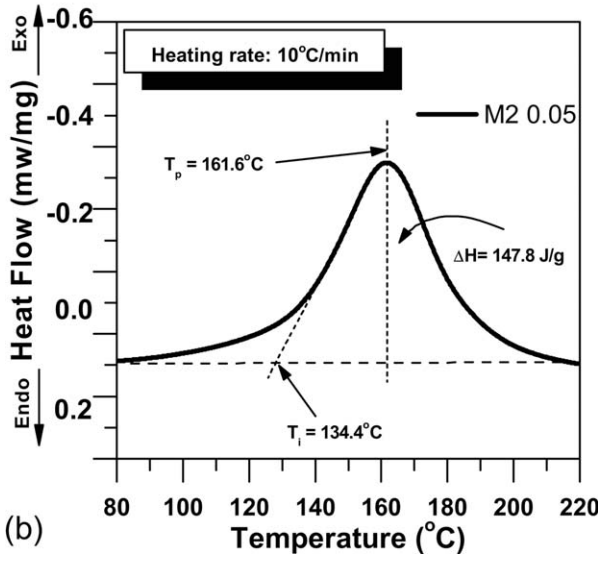

Figure 6. (a) DSC scans for M1, M2-0.05, M2-0.5, M2-1.0 and M3 (heating rate 10°C/min) (b) DSC scan of the M2-0.05 sample. [Color figure can be viewed in the online issue, which is available at wileyonlinelibrary.com.]

conductivity. The percolation threshold, which ensures the presence of a thermally conductive network, seems to fall between 0.05 wt % and 0.5 wt % as further addition of MWCNTs did not significantly improved the conductivity. Nevertheless, we observe here a lower than expected improvement in thermal conductivity (only 15% for M2-1.0 in comparison with the unmodified epoxy). This can be explained by the high density of the functionalization of the MWCNTs; each covalent interaction between the MWCNTs and the epoxy through the functional groups acts as a scattering center and reduces the overall improvement in thermal conductivity.[38]

Influence of the Content of MWCNTs on the Thermal Degradation Process

TGA of the epoxy and the MWCNT-modified epoxy were conducted at a heating rate of 5, 10, and 15°C min^{-1} in N2

Table I. Key Features of the DSC Scans at Heating Rates of 3, 10, and 15°C/min, Respectively

	3°C/min			10°C/min			15°C/min		
	T_i (°C)	T_p (°C)	ΔH (J · g^{-1})	T_i (°C)	T_p (°C)	ΔH (J · g^{-1})	T_i (°C)	T_p (°C)	ΔH (J · g^{-1})
M1	110 ± 0.4	139.2 ± 0.7	210.6 ± 2.8	133.7 ± 0.15	160.9 ± 0.25	159.65 ± 5.1	141.2 ± 0.65	171.2 ± 0.15	145.3 ± 1
M2-0.05	110.3 ± 0.25	138.4 ± 1.55	207.5 ± 2.05	134.4 ± 0.33	161.6 ± 0.3	147.8 ± 9.2	141 ± 0.9	170.7 ± 0.16	135.4 ± 2.3
M2-0.5	105.2 ± 0.2	140.3 ± 0.15	186.95 ± 3.45	128.1 ± 0.48	157.7 ± 0.53	125.53 ± 1.3	140.3 ± 0.42	169.3 ± 0.24	128.16 ± 3.02
M2-1.0	103 ± 0.44	140.4 ± 0.17	181.833 ± 3.51	125.3 ± 0.3	158.3 ± 0.05	123.8 ± 0.5	137.2 ± 0.75	168 ± 0.5	120.85 ± 0.55
M3	110.7 ± 1.57	138.7 ± 0.11	223.133 ± 5.84	131.83 ± 0.55	161.96 ± 0.11	124.6 ± 4.33	140.23 ± 1.08	172.83 ± 0.77	157.2 ± 5.10

T_i: onset temperature of intense polymerization, T_p: maximum exothermal peak temperature, ΔH: total heat of reaction.

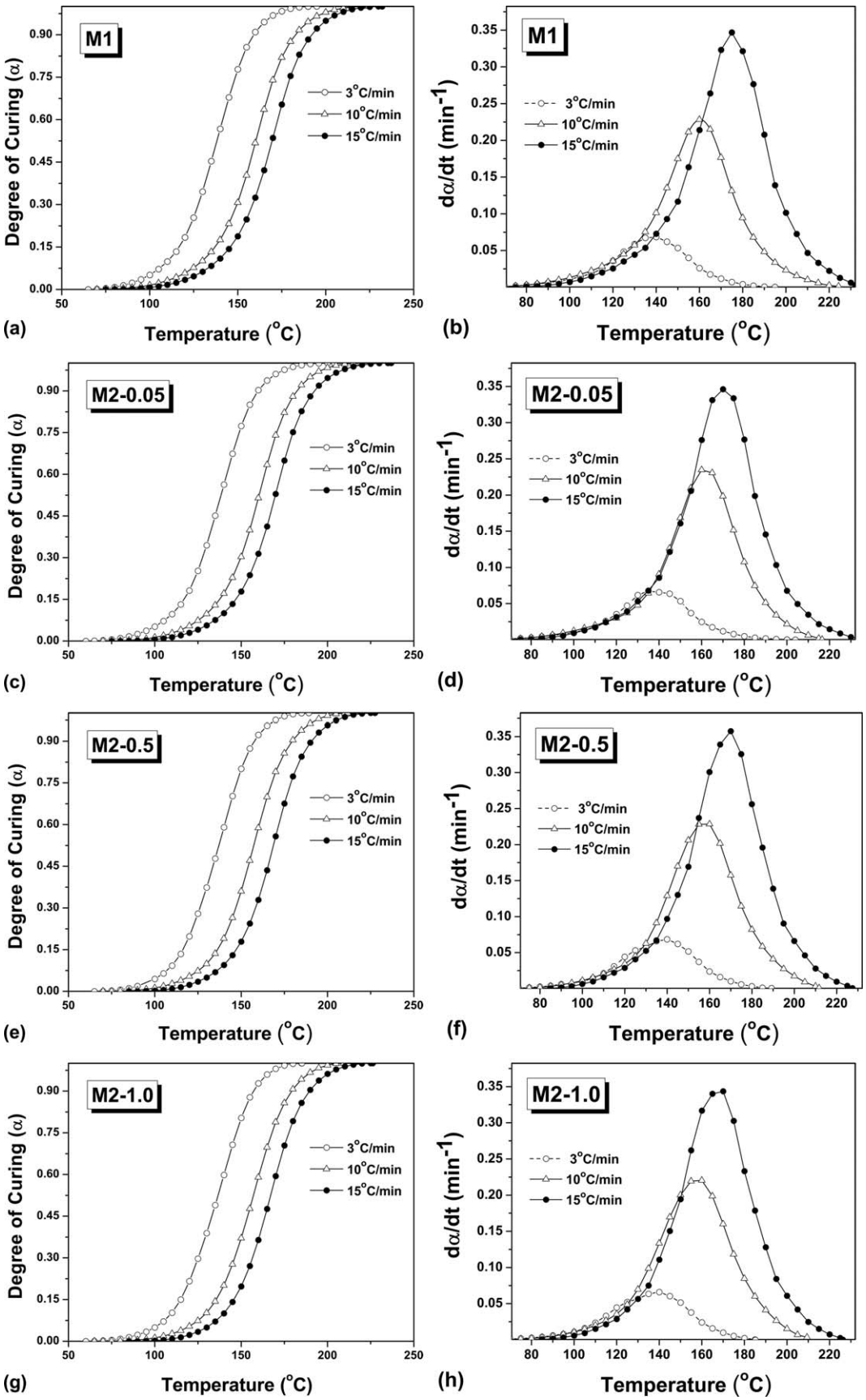

Figure 7. (a, c, e, g) Degree of conversion and (b, d, f, h) rate of conversion of the M1 and M2 samples in relations to temperature at different heating rates (3, 10, and 15°C/min).

Table II. Regression Coefficients and Apparent Polymerization Activation Energies (E_a) by the Friedman's Isoconversional Method for the Samples M1, M2 0.05, M2 0.5, and M2 1.0

α	$\ln(A \cdot f(\alpha))$ (min^{-1})	$-E_a/R$ (K)	r	E_a (kJ · mol^{-1})
M1				
0.15	14.893 ± 0.676	−7178.54 ± 283.24	0.93943 ± 0.00042	59.68 ± 2.35
0.3	15.825 ± 0.125	−7491.06 ± 107.22	0.95019 ± 0.00120	62.28 ± 0.47
0.45	17.836 ± 0.120	−8364.59 ± 41.58	0.97030 ± 0.000155	69.54 ± 0.42
0.6	20.453 ± 0.083	−9598.28 ± 108.78	0.99606 ± 0.00113	79.80 ± 0.27
0.75	21.872 ± 0.042	−10444.52 ± 22.54	0.99177 ± 0.00230	86.84 ± 0.12
0.9	21.012 ± 0.113	−10642.33 ± 50.57	0.92559 ± 0.00558	88.48 ± 0.36
M2-0.05				
0.15	17.636 ± 0.183	−8014.99 ± 152.44	0.99928 ± 0.00066	66.64 ± 1.26
0.3	19.102 ± 0.748	−8405.48 ± 102.96	0.99969 ± 0.00035	69.88 ± 0.85
0.45	20.268 ± 1.272	−9014.42 ± 187.65	0.99977 ± 0.00022	74.95 ± 1.56
0.6	19.969 ± 0.499	−9831.80 ± 234.73	0.99815 ± 0.00176	81.74 ± 1.95
0.75	18.916 ± 0.486	−9397.13 ± 29.765	0.99771 ± 0.00220	78.13 ± 0.24
0.9	7.912 ± 7.912	−8941.91 ± 608.56	0.98166 ± 0.01713	74.34 ± 5.05
M2-0.5				
0.15	17.325 ± 0.085	−8044.36 ± 39.13	0.95264 ± 0.02296	66.88 ± 0.32
0.3	19.505 ± 0.295	−8932.07 ± 114.77	0.96956 ± 0.01152	74.26 ± 0.95
0.45	20.812 ± 0.323	−9566.71 ± 129.42	0.97069 ± 0.00497	79.54 ± 1.07
0.6	20.865 ± 0.445	−9726.62 ± 182.25	0.97692 ± 0.00546	80.87 ± 1.51
0.75	20.185 ± 0.535	−9680.77 ± 223.50	0.98078 ± 0.01002	80.49 ± 1.85
0.9	17.855 ± 1.115	−9204.34 ± 482.27	0.98715 ± 0.00487	76.52 ± 4.00
M2-1.0				
0.15	17.967 ± 0.402	−8294.62 ± 162.37	0.98801 ± 0.00728	68.96 ± 1.35
0.3	19.890 ± 0.2497	−9087.11 ± 99.97	0.98982 ± 0.00592	75.55 ± 0.83
0.45	21.438 ± 0.361	−9836.88 ± 150.03	0.98656 ± 0.00576	81.78 ± 1.24
0.6	21.515 ± 0.395	−10012.43 ± 168.31	0.98660 ± 0.00572	83.24 ± 1.39
0.75	20.575 ± 0.355	−9860.36 ± 154.44	0.98771 ± 0.00555	81.98 ± 1.28
0.9	18.131 ± 0.218	−9310.32 ± 96.48	0.98639 ± 0.00916	77.41 ± 0.80

r = Correlation coefficient.

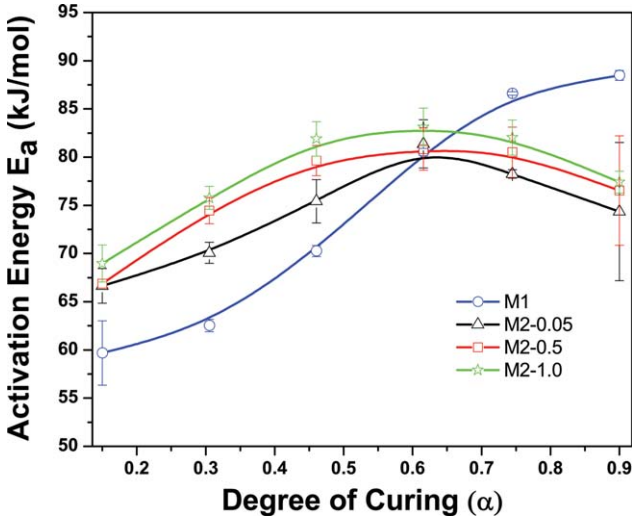

Figure 8. Evolution of E_a with the degree of conversion for all samples. [Color figure can be viewed in the online issue, which is available at wileyonlinelibrary.com.]

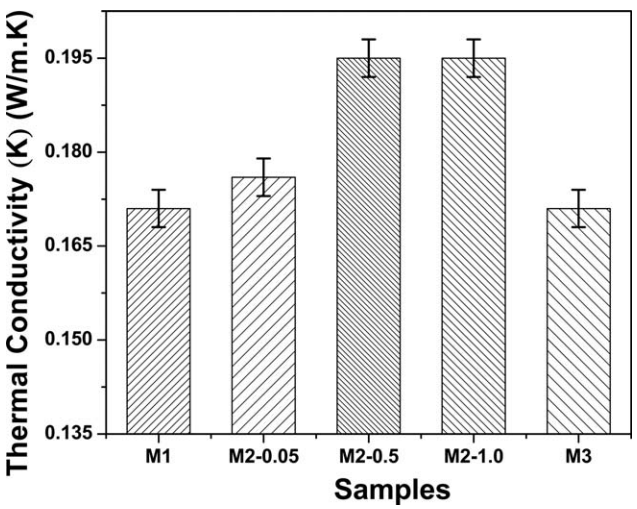

Figure 9. Thermal conductivities of the M1, M2-0.05, M2-0.5, M2-1.0, and M3 samples.

Table III. Key Features of TGA Scans for All Material Configurations at Rate 5°C/min

Sample	T_I (°C)	T_M (°C)	T_S (°C)	Residual mass (%)
M1	306.1 ± 0.5	341.7 ± 1.2	387.55 ± 0.15	9.51995 ± 0.09
M2-0.05	307.85 ± 0.85	343.55 ± 0.55	387.7 ± 0.9	10.2764 ± 0.47
M2-0.5	308.1 ± 0.3	345.6 ± 1.87	391.75 ± 2.35	10.7329 ± 0.65
M2-1.0	310.45 ± 0.25	346.55 ± 2.35	394.75 ± 2.65	11.42325 ± 0.25
M3	307.8 ± 2.8	341.15 ± 0.95	387.4 ± 0.4	10.137 ± 0.767

T_I : initial degradation temperature, T_M: peak of maximum degradation rate, T_S: temperature at which degradation stops, see Figure 10(a) for definition.

atmosphere. The thermograms of the samples, the differential thermogravimetric analysis (DTG) and the key measurements for the particular heating rate of 5°C min^{-1} are reported in Figure 10 and Table III. It can be seen that the values for T_i and T_M slightly increase with respect to CNT content Additionally, DTG analysis [Figure 10(b)] reveals that the degradation rate at peak temperature is lower for MWCNT-containing samples than for the reference configuration. These same trends are observed for the remaining heating rates.

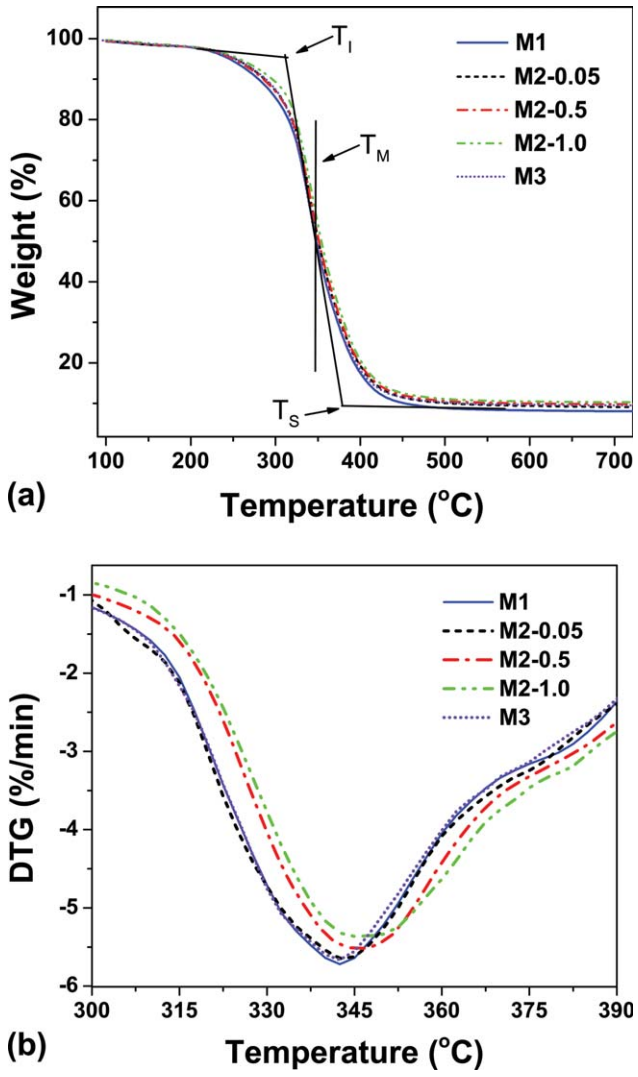

Figure 10. (a) TGA of M1, M2-0.05, M2-0.5, M2-1.0, and M3 at 5°C/min (b) Weight loss rate of all samples at 5°C/min. [Color figure can be viewed in the online issue, which is available at wileyonlinelibrary.com.]

To calculate the activation energy characteristic of the degradation process (E_d^{rd}), we used Kissinger's method, which relies on the temperature at which the maximum weight loss rate is obtained (T_M). With some rearrangement of eq. (5), the following expression is derived:

$$\frac{d\ln\left(\frac{\beta}{T_M^2}\right)}{d\ln\left(\frac{1}{T_M}\right)} = -\frac{E_d^{rd}}{R} \tag{6}$$

The value of E_d^{rd}, extracted from the plots $\ln\left(\frac{\beta}{T_M^2}\right) \leftrightarrow \frac{1000}{T_M}$ were found to be 161.32 (±10.54), 162.5 (±2.6), 168.70(±4.56), 174.93 (±2.4), and 160.11 (±7.41) kJ mol^{-1} for the M1, M2-0.05, M2-0.5, M2-1.0, and M3, respectively. The ranges of variation and regression coefficients are shown in Table IV. These results, together with the slight increase of T_i and T_M and the lower degradation rates demonstrate (1) the negligible effect of ethanol during the process and (2) the generally better thermal stability of the nano-enriched samples.[39,40]

CONCLUSIONS

Changes in the curing kinetics, thermal conductivity and thermal degradation kinetics of a EPOLAM 2063 resin system by addition of —COOH functionalized MWCNTs have been studied. Based on the experimental results and analysis, we draw the following conclusions:

- The TEM and SEM images revealed that the MWCNTs are well dispersed into the epoxy resin. A mechanism involving a covalent interaction between the —COOH group of the MWCNTs and the oxirane group of the epoxy has been suggested. The FTIR results from the cured samples confirm (1) the negligible effect of the processing conditions (including a temporary addition of ethanol) on the chemical structure; (2) a better degree of cross-linking with the complete consumption of the epoxy groups in the modified samples; and (3) the —COOH groups were not totally consumed due the reaction between the —COOH group of the MWCNTs and the oxirane group of the epoxy at the beginning of the process.
- The DSC analysis indicates that the onset temperature during curing shifted lower value with increasing MWCNT content in the epoxy. These changes occurred due to the outstanding

Table IV. Regression Coefficients and Calculated Degradation Activation Energies (E_d^{rd}) by the Kissinger Equation for the Samples M1, M2-0.05, M2-0.5, M2-1.0, and M3

Sample	$\ln((A \cdot R)/E_d^{rd})$ ($min^{-1} \cdot K^{-1}$)	$-E_d^{rd}/R \times 10^{-3}$ (K)	r	E_d^{rd}(kJ · mol^{-1})
M1	22.38 ± 3.5	19.40 ± 1.2	0.98568 ± 0.00345	161.32 ± 10.54
M2-0.05	21.14 ± 2.7	19.54 ± 0.35	0.97034 ± 0.02392	162.5 ± 2.6
M2 0.5	22.34 ± 1.4	20.29 ± 0.44	0.94651 ± 0.00628	168.70 ± 4.46
M2 1.0	23.35 ± 1.7	21.045 ± 0.28	0.97793 ± 0.01080	174.93 ± 2.4
M3	21.52 ± 3.3	19.24 ± 0.91	0.99224 ± 0.00893	160.11 ± 7.41

thermal conductivity of the MWCNTs. The polymerization activation energy (E_a) of all samples at different degrees of conversion was calculated by an isoconversional method. The higher levels of activation energy values for the M2 samples compared with the M1 samples could be explained by the reduced mobility of the epoxy chains and the unreacted groups by the increased cross-linking caused by the reaction of epoxide groups with the —COOH groups contained in the functionalized MWCNTs.

- Our thermal conductivity results confirm (1) that there was no variation between the M1 and M3 samples; (2) the thermal conductivity of cured epoxy samples improved by up to 15 % after addition of 0.5 and 1.0 wt % MWCNTs.
- Weight loss was observed in the TGA and DTG curves. The CNT-epoxy composites were found to be more thermally stable with higher degradation energy (Ed^{rd}) as the MWCNT content increased.

ACKNOWLEDGMENTS

The authors thank Mr. Chao Zhao for his support in KAUST's core facilities. The authors gratefully acknowledge financial support received from KAUST, The Boeing Company and Sabic.

REFERENCES

1. Song, Y.; Youn, J. R. *Carbon* **2005**, *43*, 1378.
2. Yuen, S. M.; Ma, C. M.; Wu, H. H.; Kuan, H. C.; Chen, W. J.; Liao, S. H.; Hsu, C. W.; Wu, H. L. *J. Appl. Polym. Sci.* **2007**, *103*, 1272.
3. Lubineau, G.; Rahaman, A. *Carbon* **2012**, *50*, 2377.
4. Liu, L.; Wagner, H. D. *Compos. Sci. Technol.* **2005**, *65*, 1861.
5. Shen, J.; Huang, W.; Wu, L.; Hu, Y.; Ye, M. *Compos. Sci. Technol.* **2007**, *67*, 3041.
6. Shen, J.; Huang, W.; Wu, L.; Hu, Y.; Ye, M. *Compos. Part A.* **2007**, *38*, 1331.
7. Chen, X.; Wang, J.; Lin, M.; Zhong, W.; Feng, T.; Chen, X.; Chen, J.; Xue, F. *Mater. Sci. Eng. A.* **2008**, *492*, 236.
8. Thostenson, E. T.; Chou, T. W. *Carbon* **2006**, *44*, 302.
9. Yeh, M.; Hsieh, T. H.; Tai, N. H. *Mater. Sci. Eng. A* **2008**, *483–484*, 289.
10. Allaoui, A.; Bai, S.; Cheng, H. M.; Bai, J. B. *Compos. Sci. Technol.* **2002**, *62*, 1993.
11. Zhan, Y.; Yang, X.; Meng, F.; Lei, Y.; Zhong, J.; Zhao, R.; Liu, X. *Polym. Int.* **2011**, *60*, 1342.
12. Jia, B.; Gao, L.; Sun, J. *Carbon* **2007**, *45*, 1476.
13. Puglia, D.; Valentini, L.; Armentano, I.; Kenny, J. M. *Diam. Relat. Mater.* **2003**, *12*, 827.
14. Xie, H.; Liu, B.; Yuan, Z.; Shen, J.; Cheng, R. *J. Polym. Sci. Part B.* **2004**, *42*, 3701.
15. Xie, H., Liu, B., Sun, Q., Yuan, Z., Shen, J., Cheng, R. *J. Polym. Sci. Part B.* **2005**, *96*, 329.
16. Choi, W. S.; Shanmugharaj, A. M.; Ryu, S. R. *Thermochim. Acta* **2010**, *506*, 77.
17. Valentini, L.; Armentano, I.; Puglia, D.; Kenny, J. *Carbon* **2004**, *42*, 323.
18. El Sawi, I., Olivier, P. A., Demont, P., Bougherara, H. *J. Appl. Polym. Sci.* **2012**, *126*, 1.
19. Wang, S.; Liang, R.; Wang, B.; Zhang, C. *Carbon* **2009**, *47*, 53.
20. Assael, M. J.; Antoniadis, K. D.; Tzetzis, D. *Compos. Sci. Technol.* **2008**, *68*, 3178.
21. Blanco, I.; Olivieri, L.; Cicala, G.; Recca, A. *J. Therm. Anal. Calorim.* **2012**, *108*, 685.
22. Abate, L.; Asarisi, V.; Blanco, I.; Cicala, G.; Recca, G. *Polym. Degrad. Stab.* **2010**, *95*, 1568.
23. Zhou, Y.; Pervin, F.; Lewis, L.; Jeelani, S. *Mater. Sci. Eng. A* **2007**, *452–453*, 657.
24. Jin, F. L.; Ma, C. J.; Park, S. J. *Mater. Sci. Eng. A* **2011**, *528*, 8517.
25. Ko, F. H.; Lee, C. Y.; Ko, C. J.; Chu, T. C. *Carbon* **2005**, *43*, 727.
26. Costa, S.; Borowiak-Palen, E.; Kruszynska, M.; Bachmatiuk, A.; Kalenczuk, R. *Mater. Sci. Poland* **2008**, *26*, 433.
27. Zou, W.; Du, Z.; Liu, Y.; Yang, X.; Li, H.; Zhang, C. *Compos. Sci. Technol.* **2008**, *68*, 3259.
28. Hong, C.; You, Y.; Pan, C. *Polymer* **2006**, *47*, 4300.
29. Friedman, H. L. *J. Polym. Sci C: Polym. Symp.* **1964**, *6*, 183.
30. Vyazovkin, S.; Burnham, A.; Criado, J.; Perez-Maqueda, L. *Thermochim. Acta* **2011**, *520*, 1.
31. Vyazovkin, S.; Sbirrazzuoli, N. *Macromol. Rapid Commun.* **2006**, *27*, 1515.
32. Kissinger, H. E. *Anal. Chem.* **1957**, *29*, 1702.
33. Cho, Y. S.; Shim, M. J.; Kim, S. W. *Mater. Chem. Phys.* **1998**, *52*, 94.

34. Park, S. J.; Kwak, G. H.; Sumita, M.; Lee, J. R. *Polym. Eng. Sci.* **2000**, *40*, 2569.

35. Lau, K.; Lu, M.; Lam, C.; Cheung, H.; Sheng, F. L.; Li, H. L. *Compos. Sci. Technol.* **2005**, *65*, 719.

36. Loos, M. R.; Coelho, L. A.; Pezzin, S. H.; Amico, S. C. *Mater. Res.* **2008**, *11*, 347.

37. Vyazovkin, S.; Sbirrazzuoli, N. *Macromolecules* **1996**, *29*, 1867.

38. Shenogin, S.; Bodapati, A.; Xue, L.; Ozisik, R.; Keblinskia, P. *Appl. Phys. Lett.* **2004**, *85*, 2229.

39. Blanco, I.; Siracusa, V. *J. Therm. Anal. Calorim.* **2012**, DOI 10.1007/s10973-012-2535-8.

40. Blanco, I.; Bottino, F. A.; Bottino, P. *Polym. Compos.* **2012**, *33*, 1903.

41. Ma, P. C.; Mo, S. Y.; Tang, B. Z.; Kim, J. K. *Carbon* **2010**, *48*, 1824.